Journal of Radiation Research and Applied Sciences 18 (2025) 101962

Contents lists available at ScienceDirect

Journal of Radiation Research and Applied Sciences

journal homepage: www.journals.elsevier.com/journal-of-radiation-research-and-applied-sciences

Design and optimization of an accelerator-based neutron source for BNCT using Geant4 Monte Carlo simulations

Reem Alanazi [a,1], Nadyah Alanazi [a,b,1], Hanan Akhdar [c], Layal Jambi [d], Abdullah N. Alodhayb [a,b,*]

[a] Department of Physics and Astronomy, College of Science, King Saud University, Riyadh, 11451, Saudi Arabia
[b] Biological and Environmental Sensing Research Unit, King Abdullah Institute for Nanotechnology, King Saud University, Riyadh, 11451, Saudi Arabia
[c] Department of Physics, College of Science, Imam Mohammad Ibn Saud Islamic University, 11623, Riyadh, Saudi Arabia
[d] Department of Radiological Sciences, College of Applied Medical Sciences, King Saud University, P.O. Box 10219, Riyadh, 11433, Saudi Arabia

A R T I C L E I N F O

Keywords:
GEANT4
Monte Carlo simulation
^{9}Be(p,n) neutron sources
BNCT
Epithermal neutrons
BSA
Collimator
Accelerator-driven

A B S T R A C T

This study investigates the generation of a neutron flux suitable for medical applications, particularly Boron Neutron Capture Therapy (BNCT). The focus was on designing a beam-shaping assembly (BSA) to moderate neutrons and distribute the flux within an aqueous water phantom. Monte Carlo simulations using the GEANT4 code were employed to model a setup in which 10 MeV proton beams interact with a beryllium target to produce fast neutrons. To moderate these neutrons to therapeutically appropriate energy levels, a layered BSA which comprises a filter, moderator, reflector, and collimator, was designed. The BSA guides neutrons through a collimator wall composed of a polyethylene slab containing lithium fluoride, with varying polyethylene concentrations of 0 %, 30 %, 50 %, 70 %, 90 %, and 100 %. The results show that replacing 50 % of the polyethylene with lithium fluoride significantly enhances neutron scattering and moderation efficiency. The neutron flux at the BSA exit port was moderated to the epithermal range required for treatment, achieving an epithermal neutron fraction of up to 93.7 % and a fluence rate of up to 5.20×10^{9} n/cm^{2}.s. The dose ratio of epithermal to fast neutron flux was 1.97×10^{-13} Gy cm^{2}/n. The dose ratio of epithermal neutrons to gamma rays was 2.40×10^{-15} Gy cm^{2}/n, while the ratio of thermal to epithermal neutron flux was 0.01. The forward directionality was 0.84, in accordance with International Atomic Energy Agency (IAEA) guidelines. Thermal neutron beam irradiation tests using the water phantom confirmed that the hydrothermal neutrons were effectively moderated and penetrated the phantom at multiple locations through the aperture, reaching 1.04×10^{9} n/cm^{2}.s at the entry and gradually decreasing along the path to 8.86×10^{8} n/cm^{2}.s at a distance of 9 cm. These results support further research into selecting the optimal configuration for treating tumors at the greatest possible depth, in the shortest treatment time, and with the most favorable therapeutic ratio.

1. Introduction

Boron neutron capture therapy (BNCT) is a cancer treatment that selectively destroys cancer cells (Saurwein et al., 2012) while causing minimal damage to surrounding healthy tissue (Cerullo et al., 2004). The method is based on boron-10 nuclei, which have a high neutron absorption cross-section and can capture low-energy neutrons within cancer cells. Once captured, boron-10 undergoes a nuclear reaction that produces alpha particles and short-range, high-energy lithium-7 nuclei (Ishikawa et al., 2024; Matsubayashi et al., 2025). The energy from these particles is deposited within the cell, destroying it with high selectivity (Zaidi, 2018). BNCT is characterized by its ability to deposit energy over distances comparable to the diameter of a single cell (Karaoglu et al., 2018), enhancing treatment precision. This makes BNCT ideally suited for treating superficial tumors, such as cutaneous melanoma. Thermal neutrons (energies below 0.5 eV) are effective in such cases, while epithermal neutrons (0.5 eV–10 keV) are more suitable for targeting deep-seated tumors (Zaidi, 2018). Until now, nuclear reactors have predominantly served as the primary means for patient trials. Yet, safety concerns and the imperative of meeting International Atomic Energy

* Corresponding author. Department of Physics and Astronomy, College of Science, King Saud University, Riyadh, 11451, Saudi Arabia.
E-mail address: aalodhayb@ksu.edu.sa (A.N. Alodhayb).
[1] These authors contributed equally to this work.

https://doi.org/10.1016/j.jrras.2025.101962
Received 8 July 2025; Received in revised form 18 August 2025; Accepted 12 September 2025
Available online 1 October 2025

Agency (IAEA) standards (Bilalodin et al., 2019) have spurred intense exploration for alternative neutron sources. These alternatives rely on accelerators (Cerullo et al., 2004). Accelerators, as noted in neutron application fields, have several potential advantages related to safety, cost, and high neutron flux in the keV range compared with reactor-based neutron sources for clinical radiotherapy (Bilalodin et al., 2019; Peng et al., 2019). Moreover, the University of Tsukuba group has initiated the construction of a ^{9}Be(p,n) neutron source driven by an 8 MeV proton accelerator (Hashimoto et al., 2015). And A ^{9}Be(p,n) accelerator-based neutron source for BNCT has recently been developed at the Research Reactor Institute, Kyoto University, Japan, utilizing a cyclotron with a proton energy of 30 MeV. While higher proton energies extend the lifetime of the beryllium target and enhance neutron production efficiency per proton, they also lead to increased radioactive byproducts, posing challenges for medical applications. In contrast, proton energies below 10 MeV significantly reduce the dose rate at the collimator bore, enabling safe operation within regulatory limits. These findings suggest that the optimal proton energy for BNCT is approximately 10 MeV, striking a balance between neutron yield and safety (Hashimoto et al., 2014; Tanaka et al., 2009a; Torres-Sánchez et al., 2021). As proton energy increases, the required beam power decreases due to higher neutron production efficiency. However, the energy spectrum of neutrons generated from the ^{9}Be(p,n) reaction shifts toward higher energies, reducing the efficiency of thermal neutron generation. For instance, the neutron yield at 30 MeV is one-third that at 8 MeV, while the thermal neutron efficiency at 8 MeV is twice that at 30 MeV. Additionally, higher proton energies result in a greater proportion of non-thermal neutrons, which are less effective for BNCT. Considering the activation of structural materials and the practicalities of maintenance, a proton energy of around 10 MeV is optimal, offering a favorable compromise between neutron production efficiency, thermal neutron yield, and system design (Sato et al., 2014).

Recent advancements in BNCT have focused on optimizing the Beam Shaping Assembly (BSA), a key component of cyclotron-based neutron sources. These systems typically utilize proton beams directed at lithium or beryllium targets to generate low-energy neutron beams. Diverse BSA configurations have been developed using advanced simulation tools such as the Monte Carlo N-Particle Transport Code (MCNP) and the Particle and Heavy Ion Transport Code System (PHITS) (Pelowitz, 2008; Sato et al., 2013). Research has also explored the design of neutron sources as a function of proton energies, ranging from 8 to 30 MeV, with intermediate materials like MgF_2, CaF_2, and AlF_3 employed to moderate neutron energy. These materials, when bombarded by neutrons, reduce the accelerator beam energy required to produce thermal neutrons at the treatment site (Kiyanagi, 2018; Nishitani et al., 2021). The primary objective is to generate neutrons within the epithermal thermal energy range of 0.5 eV–10 keV, in compliance with the quality standards set by the IAEA to determine the purity level of the epithermal beam passed from the collimator. The parameters used for evaluation include the ratio of thermal to epithermal neutron flux (ϕ_{th}/ϕ_{eip}), the gamma dose rate relative to the epithermal flux ($D_\gamma/\ \phi_{eip}$), and the fast neutron dose rate relative to the epithermal flux ($D_f/\ \phi_{eip}$). Additionally, to ensure the neutron beam is accurately focused on the treatment area and to minimize unintended radiation exposure, the neutron current-to-flux ratio ($J/\ \phi_{eip}$) is measured to assess beam divergence at the aperture exit (International Atomic Energy Agency, 2001). Generally, those accelerator-based neutron sources produce energetic neutrons typically ~ MeV range, because high doses of fast neutrons cause undesirable effects, such as damage to the irradiated skin. Moreover, it is desirable that the γ-ray component of the neutron beam is as low as possible, since the dose of γ-rays is distributed nonselectively to both tumor tissue and large volumes of healthy tissue (Hiraga, 2020) thus requiring less moderation to reach the optimal energies for BNCT, known as epithermal energies (up to 10 keV) (Torres-Sánchez et al., 2021). In order to provide a therapeutic neutron beam, a special BSA to optimize an epithermal neutron beam should be installed between the neutron source and the patient (Zaidi, 2018). It often consists of a target, a filter for fast neutrons, a moderator, a gamma-ray shield, and a neutron shield that works to reduce the size of the BSA and reduce parasitic gamma rays. (Zaidi, 2018; Nishitani et al., 2021; Monshizadeh et al., 2015).

In this work, we studied the efficiency of epithermal neutron generation and appropriate beam characteristics for BNCT based on simulation GEANT 4 high-energy physics simulation toolkits ("Geant4." Geant4) widely used to simulate neutron scattering and propagation and modeling of neutron detectors. PhysList QGSP BIC HP (which includes NeutronHPElastic, NeutronHPInelastic, Neu-tronHPCapture, NeutronHPFission) was used to simulate the interaction of neutrons with the material. In consideration of these requirements the ideal filter material was identified to moderate unwanted fast neutrons within the collimator wall region. This was achieved by varying the polyethylene concentration from 0 % to 100 % in the polyethylene-doped lithium fluoride composite within the impactor wall region. The ratios of transmitted, absorbed, and scattered neutrons relative to the incident neutrons were evaluated. Subsequently, the beam quality characteristics were analyzed to ensure compliance with requirements, along with the neutron distribution within the water phantom. To assess the neutron beam emerging from the BNCT aperture into the water phantom at varying distances, the focus is on the ability of radiation beams to penetrate the phantom. This approach aims to create a realistic experimental model and achieve a high epithermal flux.

2. Materials and methods

2.1. BSA design

Developing a neutron target system that produces neutrons via proton interactions is essential for accelerator-based compact neutron sources in BNCT. This section discusses the BSA design employing a beryllium target for the Tsukuba Group's iBNCT project (Kiyanagi, 2018; Kumada et al., 2014, 2018), a Monte Carlo simulation of the target and BSA was conducted using Geant4 (version 11.3). In the simulation, the proton source was modeled as a unidirectional circular surface source with a 7.5 cm radius, oriented along the *z*-axis, and the proton energy was set to 10 MeV (Lee et al., 2020) The source was placed 50 cm from the beamline in air, directed toward the target material. include a beryllium target system comprising a cylindrical beryllium plate (density: 1.848 g/cm^3) with a diameter of 15 cm and a thickness of 2.5 mm, which is optimal for producing neutrons with a high reproduction rate. Previous studies have identified this thickness as ideal for neutron generation from 9Be (Avagyan et al., 2017). Immediately following the beryllium layer is a palladium plate (density: 12.02 g/cm^3) with the same diameter and a thickness of 0.5 mm. This plate serves as a hydrogen absorber, capturing protons that pass through the beryllium to prevent hydrogen accumulation, which could otherwise damage the target and reduce its operational lifespan. Next is a copper block, 1 cm thick and 15 cm in diameter, embedded with cylindrical water channels a thickness of 0.3 mm. This block functions as a heat sink, dissipating the heat generated by the proton beam, thereby preventing overheating and preserving the structural stability of the system (Hashimoto et al., 2014; Kiyanagi, 2018; Kumada et al., 2018, 2023). Subsequently, the neutrons pass through a cylindrical iron (Fe) plate filter (density 7.87 g/cm^3) with a thickness of 11 cm and a length of 50.0 cm to filter the fast neutron. The neutrons then pass through a cylindrical magnesium fluoride (MgF_2) moderator, 37 cm thick and 50 cm long, with a density of 3.15 g/cm^3. MgF_2 was selected as the moderator due to its effectiveness in neutron filtering. Previous studies have shown that MgF_2 produces thermal neutrons more efficiently than other filter materials, such as CaF_2 and AlF_3. Furthermore, combining an MgF_2 moderator with Fe filters of 37 cm and 11 cm thickness, respectively, yields superior performance (Inoue et al., 2014). Studies have also indicated that MgF_2 is the optimal moderator for proton energies in the 8–10 MeV range

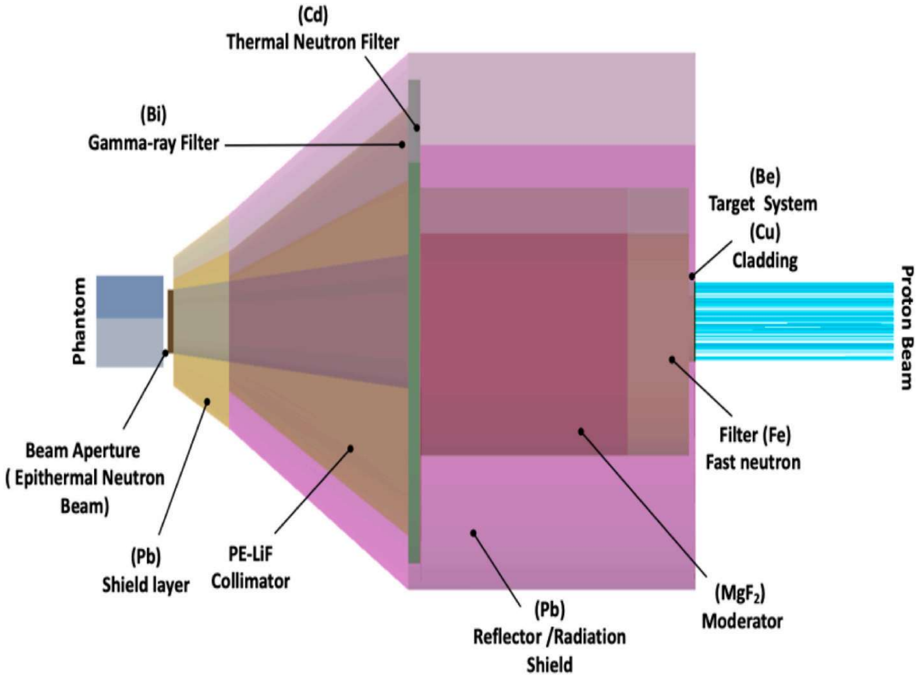

Fig. 1. Cross-section of the beam-forming assembly design, incorporating materials similar to those used in the iBNCT geometry, coupled with a 10 MeV proton beam.

(Hashimoto et al., 2015; Inoue et al., 2014). This is followed by a 0.2 cm-thick pressed cylindrical cadmium sheet to absorb thermal neutrons, and then a 2 cm-thick bismuth (Bi) sheet to filter out high-energy photons. A cylindrical collimator, which is a region where neutrons coming from bismuth (Bi) is trapped, consists of a 16 cm high of polyethylene (PE) (density 0.94 g/cm^3) blocks mixed with lithium fluoride (LiF) (density 2.639 g/cm^3) at varying concentrations (0 %, 10 %, 30 %, 50 %, 70 %, 90 %, and 100 %) of polyethylene to attenuate and capture neutrons. The collimator has a 25 cm base diameter and a 12 cm top aperture diameter. This collimator functions to reduce unwanted neutrons at the beam exit and within the patient's irradiation field. The BSA used for these simulations has a diameter of 1 m, with a 20 cm thick lead reflector enveloping the BSA completely, serving as a shield to deflect gamma rays resulting from neutron interactions as shown in Fig. 1. At the end of the collimator, a 5 cm thick lead layer is incorporated to enhance the scattering and absorption of high-energy photons generated by (n, γ) interactions in the polyethylene sheet. The simulations presented in this study do not account for shielding against secondary gamma rays absorbed by the lead in the BSA. All BSA components are positioned in direct contact with one another, eliminating any gaps between them (Inoue et al., 2014). Finally, a water brain phantom with dimensions [12 × 12 × 12] cm^3 was placed at the exit opening, positioned either directly adjacent to the opening (0 cm distance) or at distances of 3, 5, 7, and 9 cm from the BSA system, in 2 cm increments. The schematic designed BSA by using mentioned materials is shown in Fig. 1. (Bhatnagar & Sirisha, 2014; Kiyanagi, 2018; Kumada et al., 2019).

2.2. Neutron transport and interactions

Neutron interactions with matter primarily occur via scattering and absorption, which are fundamental to neutron shielding and detection (Almisned et al., 2024). For fast neutrons, scattering dominates, causing gradual energy loss through successive collisions—a process known as moderation. As neutrons slow to thermal energies (~0.025 eV), interaction probabilities increase, with absorption by heavy nuclei becoming significant. Scattering can be elastic, conserving kinetic energy, or inelastic, transferring energy to the nucleus and often resulting in gamma emission. Moderation relies chiefly on scattering to reduce neutron energies to thermal levels (Elmahroug et al., 2013; McAlister, 2016). The probability of neutron interaction is quantified by the microscopic cross-section (σ), measured in cm^2 or barns (1 b = 10^{-24} cm^2). The total microscopic cross-section (σ_t) sums elastic scattering (σ_{el}), inelastic scattering (σ_i), capture (σ_c), and fission (σ_f) cross-sections.as Eq. (1):

$$\sigma_t = \sigma_{el} + \sigma_i + \sigma_c + \sigma_f \tag{1}$$

At the macroscopic scale, the total cross-section (Σ_t) reflects the cumulative effect within a material, defined as Eq. (2) (Igwesi & Thomas, 2014):

$$\Sigma_t = N\sigma_t \tag{2}$$

where N is the atomic number density. The attenuation of a mono-energetic neutron beam passing through a material thickness x follows an exponential decay as Eq. (3) (Sahadath et al., 2015):

$$I = I_0 e^{-\Sigma_t x} \tag{3}$$

For fast neutrons, attenuation is more accurately described by the removal cross-section (Σ_r), representing the probability of the first collision removing a neutron from the uncollided flux. While Σ_r is generally less than Σ_t, it approximates Σ_t in hydrogen-rich media and is roughly two-thirds of Σ_t in materials with low hydrogen content, typically for neutron energies between 6 and 8 MeV. For compounds or mixtures, Σ_r is calculated by summing the weighted mass removal cross-sections of individual constituents as Eq. (4) (Nabil et al., 2023; Sahadath et al., 2015):

$$\Sigma_R = \Sigma_I w_i (\Sigma_R/\rho)_i \tag{4}$$

where w_i is the partial density fraction, and $(\Sigma_R/\rho)_i$ is the mass removal cross-section of constituent *i*.

The effectiveness of a moderator is best quantified by the moderating ratio (MR), defined as the ratio of macroscopic slowing-down power to macroscopic absorption cross-section. Moderation occurs via neutron collisions with nuclei, transferring kinetic energy until thermal equilibrium is reached. The fractional energy loss per collision depends on the scattering angle and the target nucleus's mass number (A); lighter

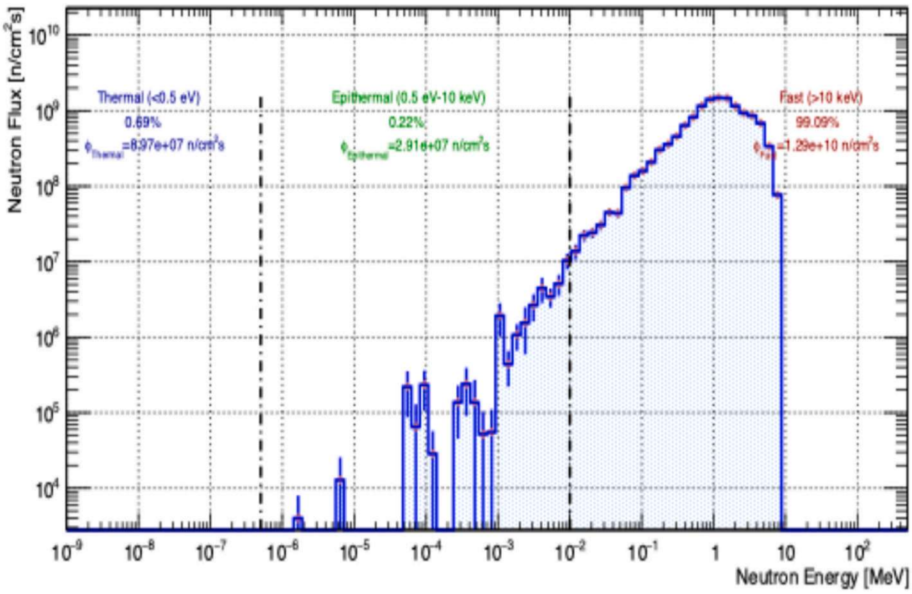

Fig. 2. Energy spectrum of neutrons emitted from a beryllium (Be) target system irradiated with a 10 MeV proton beam.

nuclei induce greater energy loss per collision. The average logarithmic energy decrement per collision, ξ, is given by as Eq. (5) (Borio et al., 2004):

$$\xi = \frac{2}{A + \frac{2}{3}} \tag{5}$$

Lighter elements exhibit higher ξ values, making them more efficient moderators. Effective moderators also require a high scattering cross-section (Σ_s) and a low absorption cross-section (Σ_a) at relevant neutron energies. Hydrogen, beryllium, and carbon are among the most effective moderators due to their optimal scattering and absorption properties and are widely used in nuclear systems. The moderating ratio (MR) is thus expressed as Eq. (6), This metric serves as a key parameter for comparing moderator materials based on their neutron slowing efficiency relative to absorption (Madbouly et al., 2018):

$$MR = \frac{\xi \Sigma_s}{\Sigma_a} \tag{6}$$

To ensure accurate representation of all neutron transport and interactions, the QGSP_BIC_HP physics list was used in Geant4 ("Geant4." Geant4) to model all relevant processes. This physics list includes elastic and inelastic scattering, capture, and fission interactions, fully covering the neutron physics required for this study. By using a tracking application, each neutron event including scattering and absorption was recorded, thereby ensuring comprehensive simulation results.

3. Results and discussion

3.1. Neutrons yield

In this section, we investigate the potential to increase neutron flux prior to moderation, as illustrated in Fig. 2. This simulation illustrates proton interactions with a beryllium target system designed to prevent proton accumulation within the beryllium plate. A secondary palladium plate is positioned behind the beryllium layer. As a hydrogen-absorbing

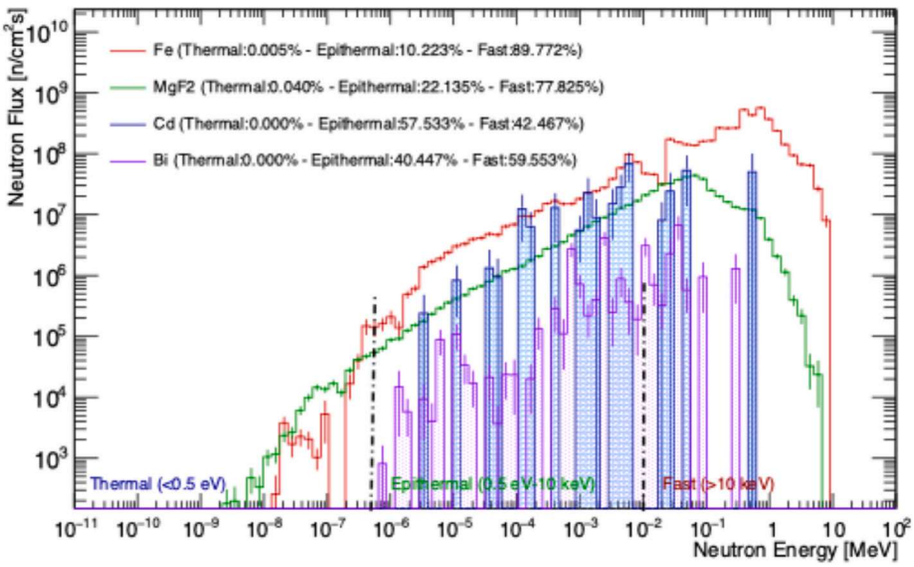

Fig. 3. Neutrons beam moderation values obtained during BSA analysis for: (1) the primary filter layer, (2) moderator layer, and (3) two secondary filter layers in the engineering design.

metal, palladium captures a significant number of protons that pass through the beryllium, thereby serving as a blister-mitigating layer. As the incident protons traverse the beryllium, they generate neutrons before coming to rest in the palladium layer. By absorbing hydrogen, the palladium helps delay blister formation and structural degradation of the beryllium target. A third copper layer is placed behind the palladium to act as a heat sink. The copper block includes internal cooling water channels to dissipate heat from all three layers. This three-layer ^{9}Be –^{46}Pd–^{29}Cu target system efficiently produces high-density neutrons, achieving a total neutron flux of approximately 10^{10} n/cm^2.s. The neutron spectrum generated by the interaction of protons with beryllium serves as a source for BSA optimization. The resulting neutron yield was calculated across an energy range with a mean energy of approximately 1.6 MeV and a maximum energy of 8 MeV. The thermal energy range accounts for 0.69 % of the total flux, corresponding to a flux of 8.97×10^7 n/cm^3.s; the epithermal energy range contributes 0.22 %, corresponding to a flux of 2.91×10^7 n/cm^3.s; and the fast energy range constitutes 99.09 %, corresponding to a flux of 1.29×10^{10} n/cm^3.s.

3.2. Moderation/attenuation of neutrons

In this study, ^{9}Be was selected as the target material for low-energy accelerator-based neutron sources, as it is commonly used when proton energies exceed 5 MeV (Dziura et al., 2023). The highest distribution of fast neutrons is found in the vicinity of the ^{9}Be target, accounting for 99.09 % of the total neutron flux, and fast neutrons spread across all components of the BSA, which do not achieve the desired treatment levels, thus cannot be used directly. The distribution of fast neutrons in the layers of BSA is shown in Fig. 3. To reduce the energy of fast neutrons to the epithermal energy range, a filter has been added. An Fe plate was positioned immediately after the beryllium target system. The filter's function is to reduce the intensity of fast neutrons before they enter the moderator. The neutron energy spectrum decreases after passing through the filter. Iron was chosen as the filter material due to its high neutron cross-section at energies above 1 MeV (Zaidi, 2018; Hashimoto et al., 2014). Most of the generated neutrons had energies averaging around 1.6 MeV, and the iron filter attenuated them, achieving a removal rate of approximately 10 %. To achieve neutrons with energies less than 1 MeV, a 37 cm thick MgF_2 plate was installed after the Fe Filter (Kiyanagi, 2018; Torres-Sánchez et al., 2021). It is essential to consider that the moderator should have a high scattering cross-section at higher energies and low absorption cross section for thermal neutrons as small as possible to avoid the loss of neutron intensity and high radiative capture reactions (Zaidi, 2018; Li et al., 2021; Bilalodin et al., 2017). In addition to the mass number, materials with a small mass number must be chosen to moderate neutrons quickly and increase thermal contamination. On the other hand, if the mass number is large, the neutrons cannot lose much of their energy per collision (Kurniawan, 2015). Given that Mg and F have average atomic masses of 24 and 19, respectively, they can modulate neutrons into the epithermal region but not into the thermal region. Additionally, 19F exhibits an inelastic collision cross-section rising from about 110 keV, making it highly effective in neutron modulation where (F) atoms play an important role in the neutron moderation process (Uritani et al., 2018).

Therefore, adopted MgF_2 as a moderator, a commonly used feedstock in BSA. The MgF_2 medium in the proton energy range from 8 MeV to 10 MeV is suitable for BSAs (Hashimoto et al., 2015). In our experiment, we used MgF_2as the moderator material. Its role is to moderate the energy of neutrons produced by protons into the energy range of thermal and epithermal neutrons without producing excessive gamma rays. Although the moderator decreases the fast neutron flux, the output neutron beam still contains thermal and fast neutrons. The neutron energy moderated by this material is more evenly distributed, with thermal neutrons constituting up to 4.96×10^8 n/cm^2.s, epithermal neutrons constituting up to 1.142×10^8 n/cm^2.s and fast neutrons accounting 3.82×10^8 n/cm^2.s of the total neutron flux. As shown in Fig. 3, the flux of fast neutrons changes after passing through the moderator, but a small percentage of unwanted thermal neutrons remains. To eliminate these, a thin cadmium plate is placed immediately after the MgF_2 medium. Our results indicate that thermal neutrons are effectively absorbed by the cadmium filter. After filtration, the thermal neutron intensity increases to 1.847×10^8 n/cm^2.s, while the fast neutron intensity decreases to 3.21×10^8 n/cm^2.s. To prevent the emission of gamma rays resulting from neutron capture reactions, a bismuth (Bi) sheet is used to absorb them (Bilalodin et al., 2019; Peng et al., 2019). Additionally, a lead layer is included in the BNCT system for gamma radiation shielding. After passing through the filter, moderator, and additional filtering stages. only 47.6 % of the simulated epithermal neutrons retained a flux of up to 1.26×10^7 n/cm^2, while 52.4 % of the fast neutrons retained a flux of 1.39×10^7 n/cm^2.s upon exiting the Bi layer. The primary focus in the BSA design was to minimize the flux of high-energy neutrons to the lowest possible level. Once the neutron spectrum is adequate to converge the neutrons to a range for BNCT, the focus shifts to shaping and collimating the beam to decrease dose delivery to healthy tissue and minimize neutron and gamma contamination off-beam. Beam shaping and focusing are achieved through a tapered geometry toward the beam aperture. This is accomplished by contracting the BSA beam port to a flat circular surface known as a collimator, surrounded by a lead reflector. Neutrons enter the collimator and are reflected off its walls, which are lined with LiF doped with PE at varying concentrations. Comparisons were made between these concentrations, and the effectiveness of the differences in moderating neutrons within the collimator region was assessed qualitatively. Neutron interactions with fluorine (F) in LiF enhance fast neutron moderation, as fluorine has a relatively large scattering cross-section for fast neutrons, this leads to an increase in the number of epithermal neutrons, it leads to an increase in the number of epithermal neutrons, which are distributed throughout the collimator with relatively high intensity. However, the intensity decreases as the neutrons pass through and interact with the collimator walls, where some are further moderated into thermal neutrons. Consequently, the thermal neutron flux intensity at the nozzle increases by approximately 1.45 %. The fast neutron intensity also decreases due to interactions with hydrogen atoms in the polyethylene, reaching a flux of 4.76 %. We found that the epithermal neutron flux at the end of the collimator is approximately greater than 10^9 n/cm^2.s, as noted in Section 3.4.

3.3. Neutron moderation in the collimator region

As a next step in the simulation, we investigated neutron moderator within the collimator region. Neutrons emitted by bismuth (Bi) enter this region with energy levels outside the desired interaction range, making them more difficult to process and rendering them unusable for the intended application. To reduce the energy of fast neutrons to the epithermal range and eliminate thermal neutron contamination, we examined various concentration ratios of polyethylene (PE) doped with lithium fluoride (LiF). PE concentrations ranging from 0 % to 100 % were evaluated to assess the effectiveness of the collider design. This analysis is essential for minimizing beam broadening and ensuring efficient neutron delivery from the BNCT system to the patient with minimal intensity loss. We evaluated how a 16 cm LiF–PE layer applied to the collimator wall affected thermal, epithermal, and fast neutron fluxes. An effective neutron moderator must scatter high-energy neutrons efficiently, exhibit low thermal neutron absorption, and minimize intensity loss. Polyethylene, a widely used thermoplastic polymer with applications across various fields, was selected as an excellent neutron moderator. It is particularly effective in shielding and moderation due to its high neutron scattering capacity (Bilalodin et al., 2020; Ivakhin et al., 2012; Osawa et al., 2017; Park et al., 2014; Zhang, Yang, et al., 2017). due to its high hydrogen content, which makes it proficient at slowing down fast neutrons. It successfully absorbs and attenuates neutrons by scattering them, thereby enabling other materials with large neutron

Table 1
Neutron Interaction Types: Percentages of transmittance, absorption, and scattering for varying concentrations of lithium fluoride-loaded polyethylene within the collimator, along with the corresponding total neutron flux at each concentration.

Compound PE (%)	Density (g/cm^3)	Mass Attenuation μ_m (cm^2/g)	Interaction Types			$\sum_R$ (cm^2/g)	Total Neutron Flux × 10^9 (n/cm^2.s)
			Transmitted (%)	Absorbed (%)	Scattered (%)		
0	2.635	0.045	14.60	0.002	75.80	0.0011	0.89648
10	2.465	0.064	7.736	0.015	78.29	0.0027	1.01667
30	2.126	0.082	6.023	0.050	80.86	0.0061	1.33078
50	1.787	0.100	5.633	0.091	82.61	0.0094	1.57653
70	1.448	0.126	5.381	0.175	84.35	0.0128	1.79434
90	1.109	0.170	4.877	0.379	87.39	0.0161	2.06764
100	0.940	0.223	3.449	0.710	91.56	0.0178	2.80385

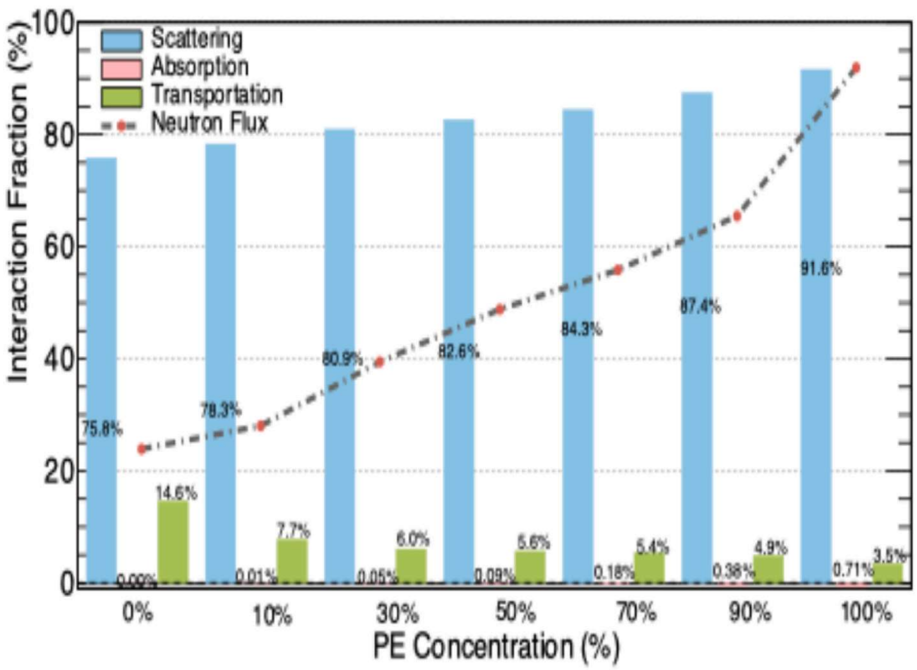

Fig. 4. Effect of varying concentrations of lithium fluoride-loaded polyethylene on transmittance, absorption, and scattering factors, as well as the resulting total neutron flux.

capture cross-sections to absorb the neutrons (Zaidi, 2018), LiF is an alkali halide that appears as a solid white powder. It contains lithium-6 (^{6}Li), which has a natural abundance of 7.5 %. ^{6}Li has a large absorption cross-section of up to 940 b for thermal neutrons, with the absorption primarily occurring without generating gamma rays. As a result, ^{6}Li is commonly used for neutron thermal shielding in medical and biological applications (Lone et al., 1980; Sakurai et al., 2004). Additionally, the fluoride component (^{19}F) of LiF has an inelastic collision scattering cross-section, allowing it to modulate neutrons very effectively (Uritani et al., 2018). LiF is particularly promising because it effectively captures neutrons with low energies (less than 10 eV) and reduces the number of neutrons with energies higher than approximately 10 keV. Therefore, LiF is very promising for enhancing shielding effectiveness in applications that require the energy range of epithermal neutrons see Table 1 (Tymińska, 2009).

Table 2
Neutron flux distributions across energy regions for varying concentrations of lithium fluoride-loaded polyethylene.

Compound PE (%)	Thermal Region (<0.5 eV)		Epithermal Region (0.5 eV–10 keV)		Fast Region (>10 keV)	
	$\phi_{Thermal}$ × 10^8 (n/cm^2.s)	(%)	$\phi_{Epithermal}$ × 10^9 (n/cm^2.s)	(%)	ϕ_{Fast} × 10^6 (n/cm^2.s)	(%)
0	0	0	0.882	98.36	14.670	1.637
10	0.166	1.63	0.995	97.87	5.000	0.491
30	1.061	7.97	1.221	91.78	3.168	0.238
50	2.336	14.82	1.340	85.01	2.538	0.160
70	3.917	21.83	1.400	78.02	2.433	0.135
90	6.569	31.77	1.408	68.11	2.318	0.112
100	10.405	50.14	1.395	49.77	2.281	0.081

We focused on measuring epithermal neutrons (0.5 eV $<$ E$_n$ $<$ 10 keV) emitted from the aperture and absorbed by the phantom. For each PE concentration, we analyzed neutron transmittance, absorption, and scattering to evaluate energy distribution changes. The results showed that transmittance increased with material density, rising from 3.44 % at 0.94 g/cm^3 to 14.60 % at 2.635 g/cm^3. Absorption remained relatively stable; it has no significant effect from 0.002 % to 0.71 %. Scattering dominated the interactions (75.80 %–91.56 %) but declined with increasing density. Similarly, the mass attenuation coefficient increases from 0.045 cm^2/g to 0.223 cm^2/g over the same density range. The study also explored neutron transmission and scattering in PE-LiF composites. As shown in Fig. 4, neutron transmission it increases with LiF concentration, following an exponential trend (Eqs. (1)–(3)), while total neutron flux decreased with reduced polyethylene content—highlighting PE's role as scatterer. A higher PE proportion significantly enhanced neutron scattering, improving overall neutron attenuation and flux. Fig. 4 illustrates the neutron flux attenuation for

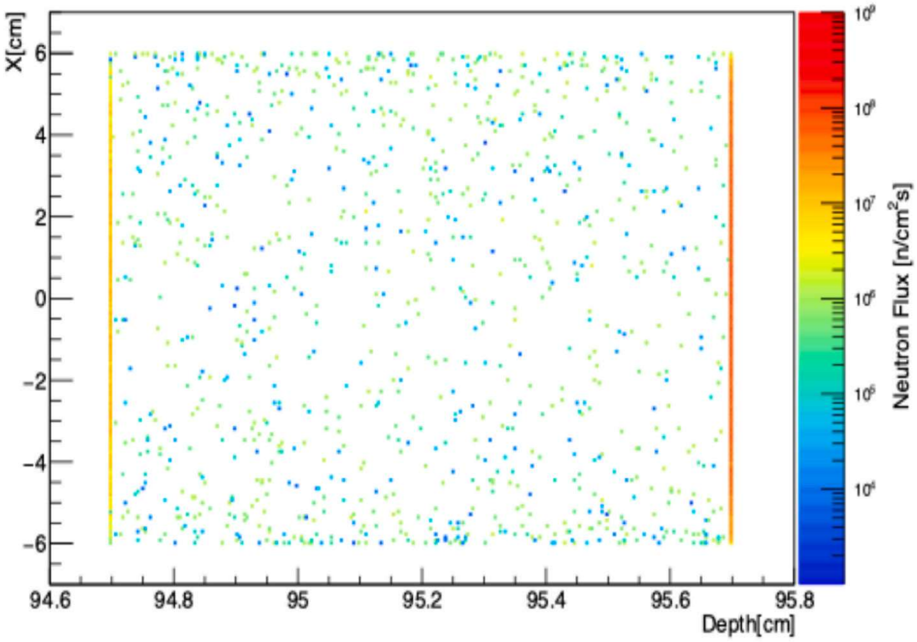

Fig. 5. The neutron flux distribution along the radial direction at the end of the collimator, where the flux is centered at the beam aperture exit.

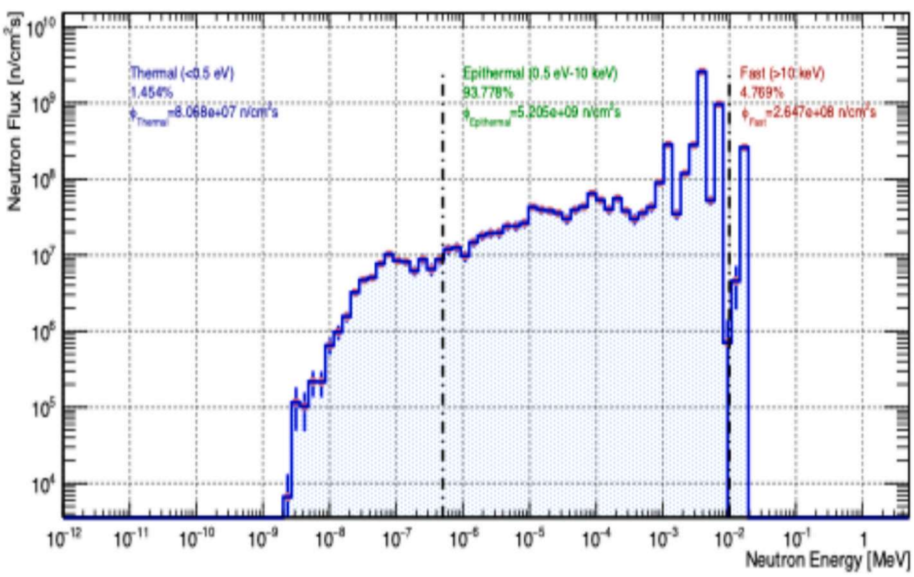

Fig. 6. Neutron energy spectrum at the BSA beam exit, highlighting the increased epithermal neutron flux intensity within the beam spectrum.

various PE and LiF concentrations. The impact on BNCT neutron beam quality is evident in the <0.5 eV range, representing thermal neutron contamination. At 50 % PE, the thermal fraction is 14.82 %, an acceptable level compared to 50.14 % at 100 % PE, which leads to excessive surface dose and reduced penetration depth. ^{6}Li in LiF absorbs thermal neutrons, thereby limiting superficial dose while maintaining sufficient thermal flux (~14.82 %). At 50 % PE, the surface epithermal neutron flux peaks at 1.340×10^9 n/cm^2·s (85.01 %), which is optimal for deep tumor penetration. This flux decreases with higher PE concentrations—78.02 % at 70 % PE, and 49.77 % and 68.11 % at 90 % and 100 % PE, respectively. In contrast, fast neutron contamination (>10 keV) is highest at 0 % PE (1.637 %) due to poor neutron moderation and lowest at 50 % PE (0.160 %), where effective moderation minimizes damage to healthy tissue. These results confirm that a 50 % PE–LiF composition provides the most effective balance, which meets the required criteria (Murata et al., 2023), as summarized in Table 2.

3.4. Neuron energy spectrum at the beam aperture

We present an overview of the neutron spectrum obtained at the BSA design aperture, which exhibits the characteristic features of the calculated neutron beam. The spectrum is broad, and the neutron beam exiting the aperture consists primarily of three types of neutrons: thermal, epithermal, and fast. The low-energy tail of the spectrum is effectively suppressed, resulting in a neutron distribution that peaks at approximately ~4 keV. This peak lies within the epithermal energy range (0.5 keV–10 keV) (Fauzi et al., 2018; Hashimoto et al., 2015). To ensure optimal performance, the neutron source must produce a high density of epithermal neutrons at the beam aperture as Fig. 5, with minimal contamination from fast neutrons and gamma rays. The neutron beam exiting the aperture is dominated by epithermal neutrons. Specifically, the fast and thermal neutron fluxes account for 4.76 % and 1.45 %, respectively, while the epithermal neutron flux constitutes up to

Table 3
Results of all parameters simulated in Geant4 at the beam aperture, along with a comparison of the in-air parameters obtained in this study with the recommended BNCT air parameters from the IAEA (IAEA-TECDOC-1223, 2001) (International Atomic Energy Agency, 2001).

Parameter	Notation	IAEA Recommendation	Collimator Output
Epithermal Neutron Flux (n/cm^2.s)	ϕ_{epi}	$>1 \times 10^9$	5.20×10^9
Fast Dose Rate/Epithermal Neutron Flux (Gy.cm^2/n)	$\frac{\dot{D_f}}{\phi_{epi}}$	$\leq 2 \times 10^{-13}$	1.97×10^{-13}
Gamma Dose Rate/ Epithermal Neutron Flux (Gy.cm^2/n)	$\frac{\dot{D_\gamma}}{\phi_{epi}}$	$\leq 2 \times 10^{-13}$	2.40×10^{-15}
The ratio of Thermal and Epithermal Neutron Flux	$\frac{\phi_{th}}{\phi_{epi}}$	<0.05	0.01
The ratio of Neutron Current and Neutron Flux	$\frac{J}{\phi_{epi}}$	>0.70	0.84

93.77 %. The spectrum exhibits well-defined peaks within the desired surface epithermal range, as illustrated in Fig. 6. To evaluate the neutron beams at the BSA design ports, we compared them with the IAEA recommended values (International Atomic Energy Agency, 2001; Zhang, Wu, et al., 2017), Zhang, Wu, et al., 2017s listed in Table 3. This table outlines the IAEA guidelines for BNCT, including the recommended neutron beam energy limits at the BSA beam exit. In the table, fast neutron flux, epithermal neutron flux, thermal neutron flux, fast neutron dose, and gamma ray dose are denoted by ϕ_{fast}, ϕ_{epi}, ϕ_{th}, D_{fast} , and D_γ, respectively. We also calculated the epithermal neutron flux (ϕ_{epi}), the ratio of thermal to epithermal neutron flux (ϕ_{th}/ ϕ_{eip}),

the ratio of fast neutron dose to epithermal neutron flux (D_{fast}/ ϕ_{epi}), and the ratio of gamma dose to epithermal neutron flux (D_γ/ ϕ_{epi}). Additionally, the total neutron flux (ϕ_{total}) and other relevant parameters at the beam exit port in air were determined. The collimator is designed to limit neutron beam divergence, reduce unintended irradiation, and focus the beam on the patient treatment area. To assess beam divergence, we calculated the fraction of the beam traveling in the forward direction, expressed as the forward current-to-flux ratio (J/ ϕ_{epi}). The final current-to-flux ratio at the orifice exit level was confirmed to be within the permissible range as Fig. 6. Simulation results confirm that the system produces a high-quality epithermal neutron flux suitable for BNCT applications, with a beam spectrum that closely matches the predictions from the design phase. As shown in Table 3, the BSA air beam parameters fully meet all IAEA-recommended standards, ensuring clinical applicability. Moreover, the system achieves the highest reported nozzle epithermal neutron flux efficiency among comparable designs with similar source energy, target material, and BSA configuration (Dziura et al., 2023; Hashimoto et al., 2014; Kumada et al., 2014, 2019, 2023; Sato et al., 2014). These findings validate the accuracy of the design methodology and underscore the superior performance of the proposed configuration, highlighting its potential to enhance BNCT treatment efficacy.

3.5. Neutron flux distributions in the phantom

We studied the neutron intensity just outside the beam extraction area of the nozzle at distances of 0, 3, 5, 7, and 9 cm from the center by placing a water phantom adjacent to the beam exit. The distribution of thermal neutrons in the water was recorded both along and perpendicular to the beam direction where the flux peaked approximately in the middle of the phantom, as illustrated in Fig. 7. A water phantom is typically chosen as a test material because approximately 70 % of the human body is composed of water. The calculated epithermal neutron flux at the end of the collimator exceeded 10^9 n/cm^2.s. Upon entering the phantom, the neutron flux began to decrease steadily in energy due to interactions with hydrogen atoms (Bilalodin et al., 2019). The values varied, with thermal neutron flux reaching up to 41 % of (7.88×10^8–1.05×10^8) n/cm^3.s and epithermal neutron flux comprising about 58 % of (1.04×10^9–8.86×10^8) n/cm^3.s. For fast neutrons, the flux dropped to just 0.09 % compared to the value at the beam exit, as shown in Fig. 8. All measurements were performed under the same conditions. The phantom was placed directly at the beam aperture exit to account for beam divergence, which can increase the irradiation area and treatment duration, potentially raising the dose to surrounding healthy tissue as the aperture size increases. Thus, the phantom placement was selected to validate the beam model in terms of flux distribution. Based on these results, the BSA-moderated neutron beams in this study can be considered suitable sources for BNCT, as the actual beam spectrum closely matches the predictions made during the design phase of the iBNCT accelerator parameters described above. This study measured neutron beam characteristics and evaluated how the epithermal neutron

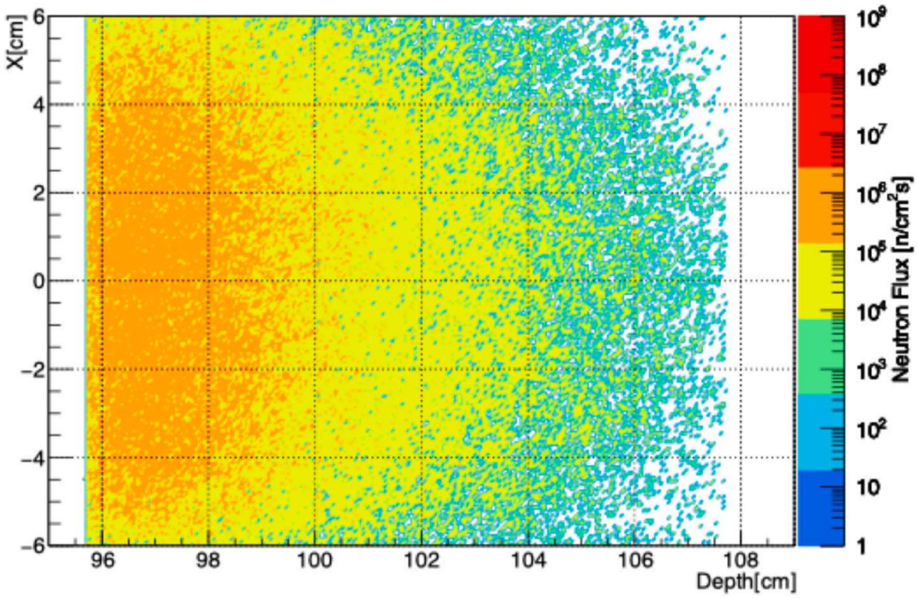

Fig. 7. Spatial mapping of neutron flux (right, in n/cm^2.s) along the beam axis in the phantom for a 12 cm beam collimator shows an elliptical distribution with a 6 cm radius along the y-axis.

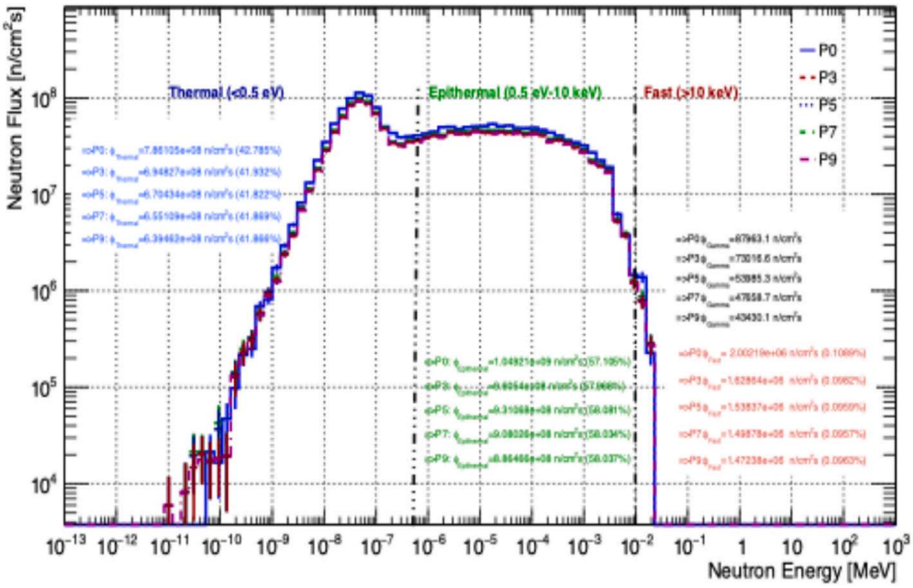

Fig. 8. Neutron flux distributions for thermal, epithermal, and fast neutrons within the phantom at various positions.

flux varies with spatial distribution in a water phantom simulating the human body measurements that are essential for accurate dose estimation in future clinical studies. However, this work did not investigate the biological effects of the simulated neutron beam, nor did it provide complete calculations of clinical parameters for direct clinical comparison, as application studies are still ongoing (Sato et al., 2024a, 2024b; Tanaka et al., 2009b).

4. Conclusion

In this study, the Geant4 Monte Carlo toolkit was employed to design BSA for the iBNCT accelerator, calculate neutron fluxes from the ^{9}Be(p, n) reaction, and evaluate neutron beam quality at the BSA exit. The design satisfied the performance criteria outlined in IAEA. Optimization focused on the effect of collimator material composition on neutron moderation. The BSA featured a conical collimator wall composed of LiF doped with PE at concentrations from 0 % to 100 %. Increasing PE content enhanced the moderation of fast neutrons into the epithermal range, increasing ϕ_{epi}. However, beyond a certain PE concentration, epithermal neutron losses to the thermal range outweighed the gains, causing a gradual decrease in ϕ_{epi}. The optimal epithermal neutron flux (5.20×10^9 n/cm^2.s at 50 % PE) was higher than that achieved in comparable designs. Additionally, evaluation of the epithermal neutron flux distribution along the *z*-axis within the water phantom from the beam opening to a depth of 9 cm showed that at a flux of 8.86×10^8 n/cm^2.s, the beam still met the required standards. The measured flux at the epithermal beam nozzle demonstrates the feasibility and potential effectiveness of the designed beam for immediate treatment of deep brain tumors. Future work will extend the Geant4 simulations to deep-brain tumor scenarios, with the aim of integrating neutron radiotherapy with boron-based drugs for the treatment of resistant and recurrent cancers, ensuring that Monte Carlo simulations yield realistic performance predictions for this device.

CRediT authorship contribution statement

Reem Alanazi: Writing – original draft, Validation, Formal analysis, Conceptualization. **Nadyah Alanazi:** Writing – review & editing, Writing – original draft, Investigation, Formal analysis. **Hanan Akhdar:** Writing – review & editing, Methodology, Investigation, Formal analysis. **Layal Jambi:** Writing – review & editing, Methodology, Data curation. **Abdullah N. Alodhayb:** Conceptualization, Writing – review, Validation, Formal analysis, Supervision.

Acknowledgement

Authors acknowledge Research Institute/Center Supporting Program (RICSP-25-1), King Saud University, Riyadh, Saudi Arabia.

References

Almisned, G., Susoy, G., & Tekin, H. O. (2024). Neutron transmission analysis in borated polyethylene, boron carbide, and polyethylene: Insights from MCNP6 simulations. *Radiation Physics and Chemistry, 218*, Article 111585. https://doi.org/10.1016/j.radphyschem.2024.111585

Avagyan, R., et al. (2017). Study of low energy neutron beam formation based on GEANT4 simulations. *Nuclear Instruments and Methods in Physics Research Section B: Beam Interactions with Materials and Atoms, 402*, 247–250. https://doi.org/10.1016/j.nimb.2017.03.091

Bhatnagar, S., & Sirisha, S. N. L. (2014). Geant4 - Study of dose curve parameters of tumor in human tissues using passive proton beam. In *2014 international conference on computational intelligence and communication networks* (pp. 178–185). IEEE. https://doi.org/10.1109/CICN.2014.50.

Bilalodin, B., et al. (2019). Characteristics in water phantom of epithermal neutron beam produced by double layer beam shaping assembly. *ASEAN Journal on Science and Technology for Development, 36*(1), 9–12. https://doi.org/10.29037/ajstd.519

Bilalodin, B., et al. (2020). ANALYSIS OF PARTICLE DISTRIBUTION IN a DOUBLE LAYER BEAM SHAPING ASSEMBLY RESULTED FROM 30 MEV-PROTON REACTIONS WITH BERYLLIUM TARGET USING THE PHITS PROGRAM. *Jurnal Teknologi, 82*(3). https://doi.org/10.11113/jt.v82.13162. Penerbit UTM Press. Crossref.

Bilalodin, B., Kusminarto, K., Hermanto, A., Sardjono, Y., & Sunardi, S. (2017). Double layer collimator for BNCT neutron source based on 30 MeV cyclotron. *Indonesian Journal of Physics and Nuclear Applications, 2*(3), 124–127. https://doi.org/10.24246/ijpna.v2i3.124-127

Borio, A., Cagnazzo, M., Marchetti, F., Pappalardo, P., & Salvini, A. (2004). Moderating ratio parameter evaluation for different materials by means of Monte Carlo calculations and reactivity direct measurements. In *Proceedings of the 2nd world TRIGA users conference* (pp. 177–182). INIS-AT-0076.

Cerullo, N., et al. (2004). Spectrum shaping assessment of accelerator-based fusion neutron sources to be used in BNCT treatment. *Nuclear Instruments and Methods in Physics Research Section B: Beam Interactions with Materials and Atoms, 213*, 641–645. https://doi.org/10.1016/S0168-583X(03)01671-9

Dziura, D., Tabbassum, S., MacNeil, A., Maharaj, D. D., Laxdal, R., Kester, O., Pan, M., Kumada, H., & Marquardt, D. (2023). Boron neutron capture therapy in the new age of accelerator-based neutron production and preliminary progress in Canada. *Canadian Journal of Physics, 101*(8), 363–372. https://doi.org/10.1139/cjp-2022-0266

Elmahroug, Y., Tellili, B., & Souga, C. (2013). Calculation of fast neutron removal cross-sections for different shielding materials. *International Journal of Physics and Research, 3*(2), 7–16.

Fauzi, A., Afifah, T. H., Ahmad, F. H., & Sutresna, W. G. (2018). Beam shaping assembly optimization for boron neutron capture therapy facility based on cyclotron 30 MeV as neutron source. *ASEAN Journal on Science and Technology for Development, 35*(3), Article 2. https://doi.org/10.29037/ajstd.536

"Geant4." *Geant4*, geant4.web.cern.ch.: https://geant4.web.cern.ch/.

Hashimoto, Y., et al. (2014). Effects of proton energy on optimal moderator system and neutron-induced radioactivity of compact accelerator-driven 9Be(p,n) neutron sources for BNCT. *Physics Procedia, 60*, 332–340. https://doi.org/10.1016/j.phpro.2014.11.045

Hashimoto, Y., et al. (2015). Optimal moderator materials at various proton energies considering photon dose rate after irradiation for an accelerator-driven 9Be(p,n) boron neutron capture therapy neutron source. *Applied Radiation and Isotopes, 106*, 88–91. https://doi.org/10.1016/j.apradiso.2015.07.027

Hiraga, F. (2020). Monte Carlo simulation-based design of an electron-linear accelerator-based neutron source for boron neutron capture therapy. *Applied Radiation and Isotopes, 162*, Article 109203. https://doi.org/10.1016/j.apradiso.2020.109203

Igwesi, D. I., & Thomas, O. S. (2014). Determination of thermal neutron macroscopic cross section for two polythene based slabs using Monte Carlo N-particle code. *Journal of Multidisciplinary Engineering Science and Technology, 1*(5).

Inoue, R., Hiraga, F., & Kiyanagi, Y. (2014). Optimum design of a moderator system based on dose calculation for an accelerator driven Boron Neutron Capture therapy. *Applied Radiation and Isotopes, 88*, 225–228. https://doi.org/10.1016/j.apradiso.2013.12.017

International Atomic Energy Agency. (2001). *Current status of neutron capture therapy*. IAEA. IAEA-TECDOC-1223).

Ishikawa, A., Tanaka, H., Nakamura, S., Kumada, H., Sakurai, Y., Watanabe, K., … Kiyanagi, Y. (2024). Effect of neutron beam properties on dose distributions in a water phantom for boron neutron capture therapy. *Journal of Radiation Research, 65* (6), 765–775. https://doi.org/10.1093/jrr/rrae076

Ivakhin, V. S., Tikhomirov, V. G., Bolozdynya, I. A., Efremenko, Y. V., Akimov, D. Y., & Stekhanov, V. N. (2012). Modeling filters for formation of mono-energetic neutron beams in the research reactor IRT MEPhI and optimization of radiation shielding for liquid-xenon detector [conference presentation]. In *Advances in reactor physics - Linking research, industry, and education (PHYSOR 2012), Knoxville, TN, United States*.

Karaoglu, A., Arce, P., Obradors, D., Lagares, J. I., & Unak, P. (2018). Calculation by GAMOS/Geant4 simulation of cellular energy distributions from alpha and lithium-7 particles created by BNCT. *Applied Radiation and Isotopes, 132*, 206–211. https://doi.org/10.1016/j.apradiso.2017.11.021

Kiyanagi, Y. (2018). Accelerator-based neutron source for boron neutron capture therapy. *Therapeutic Radiology and Oncology, 2*, 55. https://doi.org/10.21037/tro.2018.10.05

Kumada, H., et al. (2018). Development of LINAC-based neutron source for boron neutron capture therapy in University of Tsukuba. *Plasma and Fusion Research, 13*, Article 2406006. https://doi.org/10.1585/pfr.13.2406006

Kumada, H., Matsumura, A., Sakurai, H., Sakae, T., Yoshioka, M., Kobayashi, H., Matsumoto, H., Kiyanagi, Y., Shibata, T., & Nakashima, H. (2014). Project for the development of the linac based NCT facility in University of Tsukuba. *Applied Radiation and Isotopes, 88*, 211–215. https://doi.org/10.1016/j.apradiso.2014.02.018

Kumada, H., Sakae, T., & Sakurai, H. (2023). Current development status of accelerator-based neutron source for boron neutron capture therapy. *EPJ Techniques and Instrumentation, 10*, Article 18. https://doi.org/10.1140/epjti/s40485-023-00105-5

Kumada, H., Takada, K., Naito, F., Kurihara, T., Sugimura, T., Matsumoto, Y., Sakurai, H., Matsumura, A., & Sakae, T. (2019). Beam performance of the iBNCT as a compact linac-based BNCT neutron source developed by University of Tsukuba. In *AIP conference proceedings* (Vol 2160), Article 050013. https://doi.org/10.1063/1.5127705

Kurniawan, W. (2015). Optimization design of beam shaping assembly as a BNCT cancer treatment facility using D-T reaction neutron generator [Master's thesis, Program Studi Fisika FSM-UKSW]. Institutional Repository http://repository.uksw.edu/handle/123456789/10400.

Lee, S., et al. (2020). Neutron yields of Be-9(p,xn) reactions and beam characterization for accelerator-based boron neutron capture therapy facility using MCNP6, PHITS, and GEANT4 simulation results. *Nuclear Instruments and Methods in Physics Research Section B: Beam Interactions with Materials and Atoms, 478*, 233–238. https://doi.org/10.1016/j.nimb.2020.07.008

Li, G., Wu, Y., Zhang, H., Wang, X., Li, Y., & Liu, Y. (2021). Design of beam shaping assemblies for accelerator-based BNCT with multi-terminals. *Frontiers in Public Health, 9*, Article 642561. https://doi.org/10.3389/fpubh.2021.642561

Lone, M. A., Santry, D. C., & Inglis, W. H. (1980). MeV neutron production from thermal neutron capture in Li and B compounds. *Nuclear Instruments and Methods, 174*(3), 521–529. https://doi.org/10.1016/0029-554X(80)91105-2

Madbouly, A. M., & El-Sawy, A. A. (2018). Calculation of gamma and neutron parameters for some concrete materials as radiation shields for nuclear facilities. *International Journal of Emerging Trends in Engineering and Development, 4*(8). https://doi.org/10.26808/rs.ed.i8v4.02

Matsubayashi, N., Hu, N., Takata, T., Sasaki, A., Kumada, H., Nakamura, S., … Tanaka, H. (2025). Characterization of acrylic phantom for use in quality assurance of BNCT beam output procedure. *Journal of Radiation Research, 66*(1), 10–15. https://doi.org/10.1093/jrr/rrae089

McAlister, D. R. (2016). *Neutron shielding materials*. PG Research Foundation.

Monshizadeh, M., Kasesaz, Y., Khala, H., & Hamidi, S. (2015). MCNP design of thermal and epithermal neutron beam for BNCT at the Isfahan MNSR. *Progress in Nuclear Energy, 83*, 427–432. https://doi.org/10.1016/j.pnucene.2015.05.004

Murata, I., Tamaki, S., Kusaka, S., Maemunah, I. R., Sato, F., Miyamaru, H., & Yoshida, S. (2023). Neutronics design of fusion reactor-based boron neutron capture therapy in ITER. *Fusion Science and Technology, 79*(4), 465–475. https://doi.org/10.1080/15361055.2022.2151280

Nabil, I. M., El-Samrah, M. G., Omar, A., Tawfic, A. F., & El Sayed, A. F. (2023). Experimental, analytical, and simulation studies of modified concrete mix for radiation shielding in a mixed radiation field. *Scientific Reports, 13*, Article 17637. https://doi.org/10.1038/s41598-023-44978-8

Nishitani, T., et al. (2021). Neutron yield calculation of p-Li thick target by using PHITS with JENDL-4.0/HE and ENDF/B-VII for BNCT application. *Journal of Nuclear Science and Technology, 59*(5), 605–613. https://doi.org/10.1080/00223131.2021.1996297

Osawa, Y., Imoto, S., Kusaka, S., Sato, F., Tanoshita, M., & Murata, I. (2017). Development of an epi-thermal neutron field for fundamental researches for BNCT with a D-T neutron source. In *EPJ web of conferences* (Vol. 153), Article 04008. https://doi.org/10.1051/epjconf/201715304008

Park, S. J., Jang, J. G., & Lee, H. K. (2014). Computational investigation of the neutron shielding and activation characteristics of borated concrete with polyethylene aggregate. *Journal of Nuclear Materials, 452*(1–3), 205–211. https://doi.org/10.1016/j.jnucmat.2014.05.010

Pelowitz, D. B. (Ed.). (2008). *MCNPX user's manual*. Los Alamos National Laboratory.

Peng, M., He, G. Z., Zhang, Q. W., Shi, B., Tang, H. Q., & Zhou, Z. Y. (2019). Study of neutron production and moderation for sulfur neutron capture therapy. *Nuclear Science and Techniques, 30*(1), 2. https://doi.org/10.1007/s41365-018-0529-3

Sahadath, H., Kabir, K. A., Huq, M. F., & Mollah, A. S. (2015). Calculation of the different shielding properties of locally developed ilmenite-magnetite (I-M) concrete. *Radioprotection, 50*(3), 203–207. https://doi.org/10.1051/radiopro/2015005

Sakurai, Y., Sasaki, A., & Kobayashi, T. (2004). Development of neutron shielding material using metathesis-polymer matrix. *Nuclear Instruments and Methods in Physics Research Section A: Accelerators, Spectrometers, Detectors and Associated Equipment, 522*(3), 455–461. https://doi.org/10.1016/j.nima.2003.11.420

Sato, M., Fang, Z., Fukui, Y., Futatsukawa, K., Ikegami, K., Kobayashi, H., Kubota, C., Kurihara, T., Miura, T., Naito, F., Nanno, K., Obina, T., Shibata, T., Sugimura, T., Takagi, A., Kumada, H., Matsumoto, Y., Tanaka, S., Ohba, T., … Oguri, J. H. (2024a). *Status of the proton linac for boron neutron capture therapy in the iBNCT project*.

Sato, M., Fang, Z., Fukui, Y., Futatsukawa, K., Ikegami, K., Kobayashi, H., Kubota, C., Kurihara, T., Miura, T., Naito, F., Nanno, K., Obina, T., Shibata, T., Sugimura, T., Takagi, A., Kumada, H., Matsumoto, Y., Tanaka, S., Ohba, T., … Oguri, J. H. (2024b). Status of the iBNCT accelerator. *Proc. LINAC2024*, 530–534.

Sato, T., Niita, K., Matsuda, N., Hashimoto, S., Iwamoto, Y., Noda, S., … Sihver, L. (2013). Particle and Heavy Ion Transport code System, PHITS, version 2.52. *Journal of Nuclear Science and Technology, 50*(9), 913–923. https://doi.org/10.1080/00223131.2013.814553

Sato, A., Takizawa, Y., Hiraga, F., & Kiyanagi, Y. (2014). Neutron slowing down efficiency depending on the proton energy for accelerator-based BNCT. *Physics Procedia, 60*, 15–22. https://doi.org/10.1016/j.phpro.2014.11.004

Saurwein, W. A. G., Wittig, A., Moss, R., & Nakagawa, Y. (2012). *Neutron capture therapy: Principles and applications*. Springer. https://doi.org/10.1007/978-3-642-31334-9

Tanaka, H., Sakurai, Y., Suzuki, M., Masunaga, S., Kinashi, Y., Kashino, G., … Ono, K. (2009). Characteristics comparison between a cyclotron-based neutron source and KUR-HWNIF for boron neutron capture therapy. *Nuclear Instruments and Methods in Physics Research Section B: Beam Interactions with Materials and Atoms, 267*(11), 1970–1977. https://doi.org/10.1016/j.nimb.2009.03.095

Tanaka, H., Sakurai, Y., Suzuki, M., Takata, T., Masunaga, S., Kinashi, Y., Kashino, G., Liu, Y., Mitsumoto, T., Yajima, S., Tsutsui, H., Takada, M., Maruhashi, A., & Ono, K. (2009). Improvement of dose distribution in phantom by using epithermal neutron source based on the Be(p,n) reaction using a 30 MeV proton cyclotron accelerator. *Applied Radiation and Isotopes, 67*(7–8, Suppl.), S258–S261. https://doi.org/10.1016/j.apradiso.2009.03.096

Torres-Sánchez, P., et al. (2021). Optimized beam shaping assembly for a 2.1-MeV proton-accelerator-based neutron source for boron neutron capture therapy. *Scientific Reports, 11*(1). https://doi.org/10.1038/s41598-021-87305-9

Tymińska, K. (2009). Filter/moderator system for a BNCT beam of epithermal neutrons at nuclear reactor MARIA. *Polish Journal of Medical Physics and Engineering, 15*(2), 77–85. https://doi.org/10.2478/v10013-009-0008-6

Uritani, A., Watanabe, K., Hiraga, F., Fujita, K., Sakurai, Y., & Tanaka, H. (2018). Design of beam shaping assembly for an accelerator-driven BNCT system in Nagoya University. In *Journal of the Physical Society of Japan conference proceedings* (Vol. 22), Article 011002. https://doi.org/10.7566/jpscp.22.011002

Zaidi, L., et al. (2018). Beam shaping assembly design of 7Li(P,N)7Be neutron source for Boron neutron capture therapy of deep-seated tumor. *Applied Radiation and Isotopes, 139*, 316–324. https://doi.org/10.1016/j.apradiso.2018.05.029. Elsevier BVCrossref.

Zhang, F., Wu, H., Wang, X., Wu, G., Jia, W., & Ti, Y. (2017). Compact shielding design of a portable ^{241}Am-Be source. *Applied Radiation and Isotopes, 128*, 49–54. https://doi.org/10.1016/j.apradiso.2017.06.033

Zhang, X., Yang, M., Zhang, X., Wu, H., Guo, S., & Wang, Y. (2017). Enhancing the neutron shielding ability of polyethylene composites with an alternating multi-layered structure. *Composites Science and Technology, 150*, 16–23. https://doi.org/10.1016/j.compscitech.2017.06.007